In Situ Formation of Gold Nanoparticles within Thiol Functionalized HMS-C_{16} and SBA-15 Type Materials via an Organometallic Two-Step Approach

Yannick Guari,*,† Chloé Thieuleux,† Ahmad Mehdi,† Catherine Reyé,† Robert J. P. Corriu,† Silvia Gomez-Gallardo,‡ Karine Philippot,‡ and Bruno Chaudret*,‡

Laboratoire de Chimie Moléculaire et Organisation du Solide, UMR 5637 CNRS, Université de Montpellier II, Sciences et Techniques du Languedoc, Place E. Bataillon F-34095 Montpellier Cedex 5, France, and Laboratoire de Chimie de Coordination du CNRS, 205, route de Narbonne, F-31077 Toulouse Cedex 04, France

Received January 31, 2003. Revised Manuscript Received February 7, 2003

Using a two-step procedure based on (i) anchoring an organogold precursor within the channels of functionalized ordered mesoporous silica containing mercapto groups; (ii) followed by chemical reduction, we prepared materials containing gold (0) nanoparticles exclusively located within the pore channels. By modifying the organogold precursor/mercapto groups ratio, we demonstrate the necessity of the complexation of the organogold precursor prior to reduction. Using this methodology, gold content as high as 16.1 wt % with a narrow size distribution of nanoparticles regularly distributed within the pores of the material was achieved.

Introduction

Metal particles in the nanosize range represent a transition between the molecular and solid states and are therefore of great interest due to their unique properties attributed to quantum confinement or surface effects.[1] Thus, selective synthesis of such nanomaterials with well-defined size remains a significant challenge.[2] Composites of nanometer-sized metal particles with a narrow particle size distribution homogeneously dispersed in a SiO_2 matrix have been reported based on the incorporation of preformed nanoparticles within silica[3] or by sol−gel processing of the metal complex.[4] In this last case, a transition-metal-complex-containing gel is oxidized in air leading to nanosized metal oxide particles within the matrix which are then reduced under hydrogen to give metal particles. The metal dispersion and size distribution obtained by this approach depends on the kind of metal, the reaction conditions, and the metal loading.

Another approach consisted of making use of the pore channels of hexagonal mesoporous silica[5,6] as matrixes for controlling the nanoparticles size. Thus, the ordered mesoporous silica materials MCM-41,[7−11] MCM-48,[12] and FSM-16[13] have been used as templates for the growth of mono-[8−13] or bimetallic[7] transition metal nanoparticles. The general procedure used was based on impregnating the metallic precursor or grafting

* Authors to whom correspondence should be addressed. Y.G.: fax (+33) 04 67 14 38 52; e-mail guari@crit.univ-montp2.fr. B.C.: fax (+33) 05 61 33 31 00; e-mail chaudret@lcc-toulouse.fr.

† Laboratoire de Chimie Moléculaire et Organisation du Solide.

‡ Laboratoire de Chimie de Coordination du CNRS.

(1) Alivisatos, A. P. *Science* **1996**, *271*, 933. Shi, J.; Gider, S.; Babcock, D.; Awschalom, D. D. *Science* **1996**, *271*, 937.

(2) Schmid, G., Ed. *Clusters and Colloids, From Theory to Applications*; VCH: Weinheim, 1994. Feldheim, D. L.; Foss, C. A., Jr., Eds. *Metal Nanoparticles. Synthesis, Characterization, and Applications*; Marcel Dekker: New York, 2002.

(3) Khushalani, D.; Hasenzahl, S.; Mann, S. *J. Nanosci. Nanotechnol.* **2001**, *1* (2), 129. Kobayashi, Y.; Correa-Duarte, M. A.; Liz-Marzan, L. M. *Langmuir* **2001**, *17*, 6375. Selvan, S. T.; Nogami, M.; Nakamura, A.; Hamanaka, Y. *J. Nanosci. Nanotechnol.* **2001**, *1*, 129.

(4) Breitscheidel, B.; Zieder, J.; Schubert, U. *Chem. Mater.* **1991**, *3*, 559. Mörke, W.; Lamber, R.; Schubert, U.; Breitscheidel, B. *Chem. Mater.* **1994**, *6*, 1659. Lembacher, C.; Schubert, U. *New. J. Chem.* **1998**, 721.

(5) Kresge, C. T.; Leonowicz, M. E.; Roth, W. J.; Vartuli, J. C.; Beck, J. S. *Nature* **1992**, *359*, 710. Beck, J. S.; Vartuli, J. C.; Roth, W. J.; Leonowicz, M. E.; Kresge, C. T.; Schmitt, K. D.; Chu, C. T.-W.; Olsen, D. H.; Sheppard, E. W.; McCullen, S. B.; Higgins, J. B.; Schlenker, J. L. *J. Am. Chem. Soc.* **1992**, *114*, 10834. Kresge, C. T.; Leonowicz, M. E.; Roth, W. J.; Vartuli, J. C. (Mobil Oil Corp.). U.S. patent 5,098,684, **1992** [*Chem. Abstr.* **1992**, *117*, 72621]. Vartuli, J. C.; Schmitt, K. D.; Kresge, C. T.; Roth, W. J.; Leonowicz, M. E.; McCullen, S. B.; Hellring, S. D.; Beck, J. S.; Schlenker, J. L.; Olsen, D. H.; Sheppard, E. W. *Chem. Mater.* **1994**, *6*, 2317.

(6) Moller, K.; Bein, T. *Chem. Mater.* **1998**, *10*, 2950, and references therein. Ozin, G. A.; Chomski, E.; Khushalani, D.; MacLachlan, M. J. *Curr. Opin. Colloid Interface Sci.* **1998**, *3*, 181, and references therein.

(7) Ozkaya, D.; Zhou, W.; Thomas, J. M.; Midgley, P.; Keast, V. J.; Hermans, S. *Catal. Lett.* **1999**, *60*, 113. Schweyer, F.; Braunstein, P.; Estournès, C.; Guille, J.; Kessler, H.; Paillaud, H.-L.; Rosé, J. *Chem. Commun.* **2000**, 1271.

(8) Yuan, Z. Y.; Liu, S. Q.; Chen, T. H.; Wang, J. Z.; Li, H. X. *Chem. Commun.* **1995**, 973. Plyuto, Y.; Berquier, J.-M.; Jacquiod, C.; Ricolleau, C. *Chem. Commun.* **1999**, 1653.

(9) Mukherjee, P.; Patra, C. R.; Kumar, R.; Sastry, M. *Phys. Chem. Commun.* **2001**, 5. Patre, C. R.; Ghosh, A.; Mukherjee, P.; Sastry, M.; Kumar, R. *Stud. Surf. Sci. Catal.* **2002**, *141*, 641.

(10) Abe, T.; Tachibana, Y.; Uematsu, T.; Iwamoto, M. *J. Chem. Soc., Chem. Commun.* **1995**, 1617. Iwamoto, M.; Abe, T.; Tachibana, Y. *J. Mol. Catal. A: Chem.* **2000**, *155*, 143.

(11) Mulukutla, R. S.; Asakura, K.; Namba, S.; Iwasawa, Y. *Chem. Commun.* **1998**, 1425.

(12) Fröba, M.; Köhn, R.; Bouffaud, G.; Richard, O.; van Tendeloo, G. *Chem. Mater.* **1999**, *11*, 2858.

(13) Fukuoka, A.; Osada, M.; Shido, T.; Inagaki, S.; Fukushima, Y.; Ichikawa, M. *Inorg. Chim. Acta* **1999**, *294*, 281. Fukuoka, A.; Araki, H.; Sakamoto, Y.; Sugimoto, N.; Tsukoda, H.; Kumai, Y.; Akimoto, Y.; Ichikawa, M. *Nano Lett.* **2002**, *7*, 793.

10.1021/cm0213218 CCC: $25.00
Published on Web 04/15/2003

silaferrocenophanes[14] onto the support followed by calcination to generate the nanoparticles. The final size of the nanoparticles is dependent on both the pore size and the calcination temperature. Furthermore, the main problem of all these impregnation/calcination methods is the growth of nanoparticles outside the pores of silica. This problem could be circumvented in a few cases by suspending the previously impregnated material in deionized water[10] or by adding the metal salt during the material preparation.[11] However, these procedures display drawbacks: numerous washings in the first case and lack of size control in the second.

In a preliminary communication, we described a new methodology consisting of coordination of an organogold precursor within the pore channels of functionalized mesoporous silica[15] followed by metal nanoparticles growth under mild chemical reduction. Other research groups seeking cadmium sulfide[16] or gold[17] nanoparticles growth using, respectively, thiol- or amino-functionalized MCM-41 mesoporous materials have also explored this approach. This methodology should prevent outer pores growth and allow a good control of the size of the particles.[18] In this paper, we report the development and extension of this methodology. Mercapto-functionalized ordered mesoporous silica with pore sizes ranging from 21/21 to 72/59 Å (adsorption/desorption branch) are used as matrixes. These materials are prepared following the direct synthesis method, which consists of processing by the sol−gel method a solution of 3-mercaptopropyltrimethoxysilane (MPTMS) with tetraethyl orthosilicate (TEOS) in the presence of a surfactant. Following this method, the amount of organic functions incorporated, which plays a crucial role in the process leading to gold (0) nanoparticles containing materials with a narrow size distribution, can be finely tuned from 0.49 to 1.57 mmol g^{-1}. We show that the amount of gold incorporated within the materials is linked to the amount of mercapto functions and varies from 1.05 to 16.1 wt %.

Experimental Section

Reagents. (3-Mercaptopropyl)trimethoxysilane (MPTMS), tetraethyl orthosilicate (TEOS), sodium borohydride ($NaBH_4$), sodium acetylacetonate monohydrate (Na(acac), H_2O), citric acid trisodium salt ($(HOC(CO_2Na)(CH_2CO_2Na)_2)$), *n*-hexadecylamine, and Pluronic 123 ($PEO_{20}PPO_{70}PEO_{20}$ with PEO = poly(ethylene oxide) and PPO = poly(propylene oxide)) were purchased from Aldrich. Hydrogen tetrachloroaurate (III) hydrate was purchased from Strem. Chloro(tetrahydrothiophene)gold(I) (AuCl(THT)) was synthesized as described in the literature.[19] Tetrahydrofuran and ethanol were distilled and degassed before use.

Analytical Methods. Cross-polarization magic angle spinning (CP MAS) ^{29}Si NMR spectra were recorded on a Bruker FTAM 300 as were CP MAS ^{13}C NMR spectra. In both cases, the repetition time was 5 and 10 s with contact times of 5 and 2 ms. Q^n and T^n notations are given respectively for $((SiO)_n\text{-}SiO_{4-n})$ and $((SiO)_n(R)SiO_{3-n})$ environments. Specific surface areas were determined by the Brunauer−Emmett−Teller (BET) method on Micromeritics ASAP 2010 and Micromeritics Gemini III 2375 analyzers. Elemental analyses were performed by the Service Central d'Analyse (CNRS, Vernaison, France). IR spectra were recorded on a Perkin-Elmer 1600 spectrometer. UV−Visible spectra were obtained on the UV−Visible Perkin-Elmer Lambda 14 spectrometer. Powder X-ray diffraction patterns were measured on a Bruker D5000 diffractometer equipped with a rotating anode (Institut Européen des Membranes, Montpellier, France). Transmission Electron Microscopy (TEM) observations was carried out at 100 kV (JEOL 1200 EXII). Samples for TEM measurements were prepared by one of the following methods. (i) The samples were prepared using ultramichrotomy techniques and then deposited on copper grids. (ii) A drop of a suspension of the solid in ethanol was deposited on cleaved mica and followed by carbon film evaporation. This sample was then immersed in a dilute solution of HF and the recovered carbon film (replica) was deposited on copper grids. (iii) A drop of a suspension of the solid in ethanol was deposited on carbon-coated copper grid and the solvent evaporated.

Materials. All manipulations were carried out with standard high vacuum and dry-argon techniques. Functionalized materials **1**−**4** were prepared using the so-called direct method via co-condensation of the primary building blocks (MPTMS and TEOS) in the presence of the surfactant.

Material **1**. A mixture of MPTMS (85.4 mg, 0.43 mmol) and TEOS (4.55 g, 21.8 mmol) was added under stirring to 22.5 mL (60.6 mmol) of a 0.27 M solution of *n*-hexadecylamine in a 55:45 EtOH (95%)/H_2O mixture at 30 °C. A white precipitate appeared within some minutes. The reaction mixture was kept at 30 °C for 24 h. The solid was filtered, the *n*-hexadecylamine was removed by Soxhlet extraction over ethanol for 24 h, and the solid was then dried at 120 °C under vacuum.

Material **2**. **2** was prepared using the same protocol as that for **1** with MPTMS (294 mg, 1.50 mmol) and TEOS (5.94 g, 28.5 mmol).

Material **3**. We prepared functionalized hexagonally ordered mesoporous silica by hydrolysis and co-polycondensation of MPTMS (441 mg, 2.25 mmol) and TEOS (8.89 g, 42.7 mmol) in the presence of the nonionic surfactant P123 as structure-directing agent under acidic conditions at 60 °C. Our procedure was inspired by that described by Prouzet et al.[20] leading to MSU silica by using tergitol as structure-directing agent. It involves two steps: first, the formation of a micro-emulsion from the nonionic surfactant P123, MPTMS, and the TEOS under acidic conditions, then addition of a catalytic amount of fluoride (NaF; 75 mg, 1.85 mmol) ion to induce the polycondensation. ^{13}C NMR (75 MHz, CPMAS) δ: 11.5 (CH_2Si), 16.6 (CH_2CH_2Si), 27.6 (CH_2SH). ^{29}Si NMR (60 MHz, CPMAS): −57.1 (T^2), −64.7 (T^3), −90.9 (Q^2), −100.8 (Q^3), −108.9 (Q^4).

Material **4**. This was prepared using the same protocol as that for **3** with MPTMS (454 mg, 2.31 mmol) and TEOS (4.44 g, 21.3 mmol). TGA (weight loss %, [T, °C]): −18.9% [220−1200 °C]. IR (DIRFT, KBr) ν: 2576 cm^{-1} (S−H stretching).

Method A. ($^A1_{0.2}$). A suspension of **1** (200 mg) in deionized water (40 mL) was heated at reflux for 10 min. Then, a solution of $HAuCl_4 \cdot 3H_2O$ (5 mg, 0.013 mmol) in water (7 mL) was

(14) MacLachlan, M. J.; Ginzburg, M.; Coombs, N.; Raju, N. P.; Greedan, J. E.; Ozin, G. A.; Manners, I. *J. Am. Chem. Soc.* **2000**, *122*, 3878.

(15) Guari, Y.; Thieuleux, C.; Mehdi, A.; Reyé, C.; Corriu, R. J. P.; Gomez-Gallardo, S.; Philippot, K.; Chaudret, B.; Dutartre, R. *Chem. Commun.* **2001**, 1374.

(16) Wellmann, H.; Rathousky, J.; Wark, M.; Zukal, A.; Schylz-Ekloff, G. *Microporous Mesoporous Mater.* **2001**, *44*−*45*, 419.

(17) Patra, C. R.; Ghosh, A.; Mukherjee, P.; Sastry, M.; Kumar, R. *Stud. Surf. Sci. Catal.* **2002**, *141*, 641. Mukherjee, P.; Patra, C. R.; Kumar, R.; Sastry, M. *PhysChemComm* **2001**, *5*, 1.

(18) Rodriguez, A.; Amiens, C.; Chaudret, B.; Casanove, M.-J.; Lecante, P.; Bradley, J. S. *Chem. Mater.* **1996**, *8*, 1978. Bardaji, M.; Vidoni, O.; Amiens, C.; Chaudret, B.; Casanove, M.-J.; Lecante, P. *New J. Chem.* **1997**, *21*, 1. Dassenoy, F.; Philippot, K.; Ould Ely, T.; Amiens, C.; Lecante, P.; Snoeck, E.; Mosset, A.; Casanove, M.-J.; Chaudret, B. *New J. Chem.* **1998**, 703. Vidoni, O.; Philippot, K.; Amiens, C.; Chaudret, B.; Balmes, O.; Malm, J. O.; Bovin, J. O.; Senocq, F.; Casanove, M.-J. *Angew. Chem., Int. Ed.* **1999**, *38*, 3736. Pan, C.; Dassenoy, F.; Casanove, M.-J.; Philippot, K.; Amiens, C.; Lecante, P.; Mosset, A.; Chaudret, B. *J. Phys. Chem. B* **1999**, *103*, 10098. Gomez, S.; Philippot, K.; Collière, V.; Chaudret, B.; Senocq, F.; Lecante, P. *Chem. Commun.* **2000**, 1945. Soulantica, K.; Maisonnat, A.; Fromen, M.-C.; Casanove, M.-J.; Lecante, P.; Chaudret, B. *Angew. Chem., Int. Ed.* **2001**, *40*, 448.

(19) Uson, R.; Laguna, A.; Laguna, M. *Inorg. Synth.* **1989**, *26*, 85.

(20) Boissière, C.; Larbot, A.; Prouzet, E. *Chem. Mater.* **2000**, *12*, 1937.

added. The suspension was stirred (about 5 min) until the solid became yellow and the solution was colorless. Then, a solution of $HOC(CO_2Na)(CH_2CO_2Na)_2$ (50 mg, 0.194 mmol) in water (5 mL) was added to the suspension. The resulting mixture was refluxed 5 min more and filtered off. The white solid **($^A1_{0.2}$)** (153 mg) obtained was vacuum-dried at 120 °C for 12 h.

($^A2_{0.2}$), **($^A3_{0.2}$)**, and **($^A4_{0.2}$)** were prepared using the same protocol from **2** (400 mg), **3** (400 mg), and **4** (400 mg), respectively, using $HAuCl_4 \cdot 3H_2O$ (25 mg, 0.065 mmol for **($^A2_{0.2}$)** and **($^A3_{0.2}$)**; and 47 mg, 0.122 mmol for **($^A4_{0.2}$)**) and $HOC(CO_2Na)(CH_2CO_2Na)_2$ (250 mg, 0.970 mmol for **($^A2_{0.2}$)** and **($^A3_{0.2}$)**; and 500 mg, 1.94 mmol for **($^A4_{0.2}$)**).

[$^A1_{0.2}$]. A 50-mg portion of **($^A1_{0.2}$)** was suspended in 10 mL of ethanol (EtOH). A 1wt % freshly prepared solution of $NaBH_4$ in ethanol (240 μL) was added. The resulting pinkish suspension was stirred in an oil bath at 60 °C for 12 h. The solution was filtered off, and the purple solid obtained (47 mg) was vacuum-dried at 120 °C for 12 h to give **[$^A1_{0.2}$]**. **[$^A2_{0.2}$]**, **[$^A3_{0.2}$]**, and **[$^A4_{0.2}$]** were prepared using the same protocol from **($^A2_{0.2}$)**, **($^A3_{0.2}$)**, and **($^A4_{0.2}$)**, respectively.

Method B. ($^B2_{0.2}$). A suspension of **2** (200 mg) in tetrahydrofurane (THF, 15 mL) was placed in a Schlenk tube immersed in an oil bath at 60 °C. A solution of AuCl(THT) (10 mg, 0.031 mmol) in THF (5 mL) was then added, followed 15 min later by addition of a solution of $Na(acac) \cdot H_2O$ (5 mg, 0.037 mmol) in THF (5 mL). Addition of Na(acac) results in the formation of the unstable complex Au(acac)(THT), which reacts immediately with thiol groups to give the polymeric complex $-(Au^ISR)-$. The resulting suspension was stirred for 15 min more and filtered off. The white solid **($^B2_{0.2}$)** (205 mg) obtained was vacuum-dried at 120 °C for 12 h.

($^B3_{0.2}$) was prepared according to the same protocol as **($^B2_{0.2}$)** from **3** (200 mg) using AuCl(THT) (10 mg, 0.031 mmol) and $Na(acac) \cdot H_2O$ (5 mg, 0.037 mmol).

($^B3_{0.5}$) ([Au]/[SR], 0.5), **($^B3_1$)** ([Au]/[SR], 1), and **($^B3_2$)** ([Au]/[SR], 2) were also prepared using the same protocol as for **($^B3_{0.2}$)** from **3** (100 mg) using AuCl(THT) (12.5 mg, 0.039 mmol for **($^B3_{0.5}$)**; 25 mg, 0.079 mmol for **($^B3_1$)**; and 50 mg, 0.158 mmol for **($^B3_2$)**) and $Na(acac) \cdot H_2O$ (6.2 mg, 0.039 mmol for **($^B3_{0.5}$)**; 12.5 mg, 0.079 mmol for **($^B3_1$)**; and 25 mg, 0.158 mmol for **($^B3_2$)**).

($^B4_{0.77}$) was prepared using the same protocol as for **($^B2_{0.2}$)** from **4** (150 mg) using AuCl(THT) (55 mg, 0.173 mmol) and $Na(acac) \cdot H_2O$ (27.4 mg, 0.173 mmol). The suspension was stirred for 48 h instead of 15 min after addition of the reactants.

[$^B2_{0.2}$]. A 100-mg portion of **($^B2_{0.2}$)** was suspended in 10 mL of ethanol. A 2.3-mL aliquot of a freshly prepared solution of $NaBH_4$ in ethanol (0.132 M) was added. The resulting pinkish suspension was stirred in an oil bath at 60 °C for 12 h. The solution was filtered off, and the purple solid obtained was vacuum-dried at 120 °C for 12 h to give **[$^B2_{0.2}$]**. **[$^B3_{0.2}$]**, **[$^B3_{0.5}$]**, **[$^B2_1$]**, and **[$^B2_2$]** were prepared using the same protocol as for **[$^B2_{0.2}$]** from **($^B3_{0.2}$)**, **($^B3_{0.5}$)**, **($^B3_1$)**, and **($^B3_2$)**, respectively.

[$^B3_2$]. S_{BET}: 308 $m^2\ g^{-1}$. Elemental analysis calcd (%) for $C_3H_7O_{39.5}SSi_{20}Au_2$: Au 24.16, S 1.96, Si 34.45. Found: Au 19.87, S 1.53, Si 31.78; i.e. $C_3H_7O_{46.5}SSi_{23.5}Au_{2.1}$. Yield: 93%.

[$^B4_{0.77}$] was prepared as **[$^B2_{0.2}$]** from **($^B4_{0.77}$)** but stirred for 48 h after addition of $NaBH_4$ instead of 12 h.

Results and Discussion

Synthesis of Materials 1−4 and Characterization. Four materials were prepared by the co-condensation route of MPTMS with *z* equivalents of TEOS in the presence of a structure-directing agent: *n*-hexadecylamine for HS−HMS-C_{16} materials **1** ($z = 41$) and **2** ($z = 19$), and Pluronic 123 for HS−SBA-15 materials **3** ($z = 19$) and **4** ($z = 9$) (Santa Barbara n*o*. 15) (Scheme 1).[20,21]

Scheme 1. Preparation of Materials 1−4

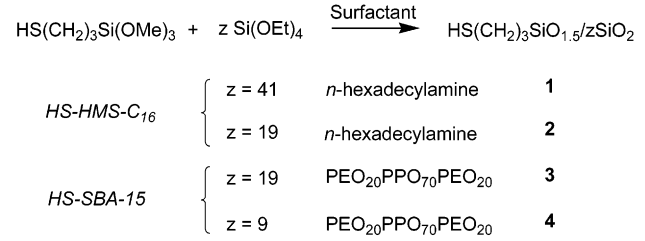

The surfactant used induces pore size going from 21/21 Å for **2** to 72/59 Å (adsorption/desorption branch) for **3** (Table 1). As the composition of the final materials is directly linked to the amount of reactants introduced, this direct synthesis method of functionalization of ordered mesoporous silica allows a strict control of the organic content incorporated within the hybrid material. Furthermore, by increasing the amount of organic

Table 1. Textural Data of the Ordered Mesoporous Materials Prepared

sample	RSi(OEt)3/TEOS	organic contents[a] (mmol g^{-1})	S_{BET} ($m^2\ g^{-1}$)	Dp[b] (Å)	Vp ($cm^3\ g^{-1}$)	d_{100} (Å)	wall thickness[c] (Å)
1	1/41	0.49	1055	23/23	0.920	45	29/29
($^A1_{0.2}$)	1/40	0.39	580	52/34	0.941		
[$^A1_{0.2}$]	1/37	0.42	535	51/39	0.889		
2	1/19	1.01	955	21/21	0.885	46	33/33
($^A2_{0.2}$)	1/18	0.82	730	27/30	0.931		
[$^A2_{0.2}$]	1/23	0.62	390	26/30	0.479		
($^B2_{0.2}$)	1/16	0.91					
[$^B2_{0.2}$]			939	-/24	0.631		
3	1/19	1.01	870	72/59	1.378	102	46/59
($^A3_{0.2}$)	1/16	0.88	520	70/50	0.582		
[$^A3_{0.2}$]	1/15	0.93	70	71/50	0.105		
($^B3_{0.2}$)			813	70/60	1.253		
[$^B3_{0.2}$]	1/29	0.53	588	72/50	0.987		
($^B3_{0.5}$)			662	73/66	1.053		
[$^B3_{0.5}$]	1/26	0.55	811	72/50	1.333		
($^B3_1$)			446	72/59	0.682		
[$^B3_1$]	1/23	0.57	494	59/51	0.836		
($^B3_2$)			430	71/52	0.691		
[$^B3_2$]	1/23	0.53	308	59/50	0.539		
4	1/9	1.57	675	53/46	0.806	92	53/60
($^A4_{0.2}$)	1/6	1.96	660	45/34	0.720		
[$^A4_{0.2}$]	1/6	2.06	270	39/34	0.392		
($^B4_{0.77}$)							
[$^B4_{0.77}$]	1/10	1.08	105	34/30	0.136		

[a] Calculated from elemental analysis. [b] Calculated from adsorption/desorption branch. [c] Calculated by a_0 − pore size (a_0 : $2d_{100}/3^{(1/2)}$).

Table 2. Elemental Analysis Data and Yields of the Ordered Mesoporous Materials Prepared

sample	elemental analysis calcd	elemental analysis found	yield
1	S 1.01, Si 45.13 for $C_3H_7O_{101.5}SSi_{51}$	S 0.99, Si 36.30 i.e. $C_3H_7O_{83.5}SSi_{42}$	100
(^{A}1$_{0.2}$)	Au 1.22, S 1.00, Si 44.58 for $C_3H_7O_{101.5}SSi_{51}Au_{0.2}$	Au 1.08, S 1.05, Si 37.10 i.e. $C_3H_7O_{82.3}SSi_{41.4}Au_{0.2}$	78
[^{A}1$_{0.2}$]	Au 1.22, S 1.00, Si 44.58 for $C_3H_7O_{101.5}SSi_{51}Au_{0.2}$	Au 1.05, S 1.14, Si 36.45 i.e. $C_3H_7O_{74.7}SSi_{37.6}Au_{0.2}$	94
2	S 2.53, Si 44.27 for $C_3H_7O_{39.5}SSi_{20}$	S 2.08, Si 36.09 i.e. $C_3H_7O_{39.1}SSi_{19.8}$	100
(^{A}2$_{0.2}$)	Au 3.01, S 2.45, Si 42.94 for $C_3H_7O_{39.5}SSi_{20}Au_{0.2}$	Au 3.45, S 2.36, Si 36.10 i.e. $C_3H_7O_{36.5}SSi_{18.5}Au_{0.2}$	58
[^{A}2$_{0.2}$]	Au 3.01, S 2.45, Si 42.94 for $C_3H_7O_{39.5}SSi_{20}Au_{0.2}$	Au 3.30, S 1.63, Si 33.30 i.e. $C_3H_7O_{48.1}SSi_{24.3}Au_{0.3}$	100
(^{B}2$_{0.2}$)	S 1.01, Si 45.13 for $C_3H_7O_{39.5}SSi_{20}Au_{0.2}$	S 0.99, Si 36.30	55
[^{B}2$_{0.2}$]			100
3	S 2.53, Si 44.27 for $C_3H_7O_{39.5}SSi_{20}$	S 2.14, Si 26.00 i.e. $C_3H_7O_{39.1}SSi_{19.8}$	100
(^{A}3$_{0.2}$)	Au 3.01, S 2.45, Si 42.94 for $C_3H_7O_{39.5}SSi_{20}Au_{0.2}$	Au 3.12, S 2.28, Si 37.42 i.e. $C_3H_7O_{37.1}SSi_{17.8}Au_{0.2}$	83
[^{A}3$_{0.2}$]	Au 3.01, S 2.45, Si 42.94 for $C_3H_7O_{39.5}SSi_{20}Au_{0.2}$	Au 3.20, S 2.56, Si 36.20 i.e. $C_3H_7O_{33.7}SSi_{17.1}Au_{0.2}$	100
(^{B}3$_{0.2}$)			99
[^{B}3$_{0.2}$]	Au 3.01, S 2.45, Si 42.94 for $C_3H_7O_{39.5}SSi_{20}Au_{0.2}$	Au 2.22, S 1.47, Si 32.82 i.e. $C_3H_7O_{58.5}SSi_{23.5}Au_{0.28}$	100
(^{B}3$_{0.5}$)			89
[^{B}3$_{0.5}$]	Au 7.20, S 2.34, Si 41.11 for $C_3H_7O_{39.5}SSi_{20}Au_{0.5}$	Au 6.73, S 1.47, Si 32.82 i.e. $C_3H_7O_{52.5}SSi_{26.5}Au_{0.75}$	100
(^{B}3$_1$)			100
[^{B}3$_1$]	Au 13.74, S 2.23, Si 39.18 for $C_3H_7O_{39.5}SSi_{20}Au_1$	Au 11.24, S 1.53, Si 33.01 i.e. $C_3H_7O_{48.1}SSi_{24.3}Au_{1.19}$	87
(^{B}3$_2$)			100
[^{B}3$_2$]	Au 24.16, S 1.96, Si 34.45 for $C_3H_7O_{39.5}SSi_{20}Au_2$	Au 19.87, S 1.53, Si 31.78 i.e. $C_3H_7O_{46.5}SSi_{23.5}Au_{2.1}$	93
4	S 4.80, Si 42.00 for $C_3H_7O_{19.5}SSi_{10}$	S 4.20, Si 33.70 i.e. $C_3H_7O_{18.1}SSi_{9.3}$	97
(^{A}4$_{0.2}$)	Au 5.56, S 4.53, Si 39.70 for $C_3H_7O_{19.5}SSi_{10}Au_{0.2}$	Au 7.70, S 5.90, Si 29.70 i.e. $C_3H_7O_{12.9}SSi_{5.7}Au_{0.2}$	63
[^{A}4$_{0.2}$]	Au 5.56, S 4.53, Si 39.70 for $C_3H_7O_{19.5}SSi_{10}Au_{0.2}$	Au 6.40, S 4.74, Si 26.20 i.e. $C_3H_7O_{12.1}SSi_{6.3}Au_{0.2}$	100
(^{B}4$_{0.77}$)			
[^{B}4$_{0.77}$]	Au 18.53, S 3.92, Si 34.31 for $C_3H_7O_{19.5}SSi_{10}Au_{0.77}$	Au 16.13, S 2.77, Si 24.74 i.e. $C_3H_7O_{21.9}SSi_{11.2}Au_{0.95}$	92

content, a decrease in the pore size is obtained from 72/59 (adsorption/desorption branch) for **3** to 53/46 (adsorption/desorption branch) for **4** (Table 1). ^{29}Si CP MAS NMR spectra of all the materials displayed resonances for siloxane (Q^n) and organosiloxane (T^n) centers with, in this last case, predominance of T^3, which is indicative of extensive condensation of the organic moiety. For all the materials prepared, results of elemental analyses, particularly for the silicium element, are lower than the expected theoretical values (Table 2). This is due to the incomplete condensation in the silica framework, which results in the presence of residual alkoxy groups as it can be concluded from the presence of T^1, T^2, Q^2, and Q^3 centers. The solid state ^{13}C CP MAS NMR spectra of these materials exhibit signals at δ 27.6 (CH_2−SH) and δ 16.6 (CH_2−CH_2−SH) in addition to a slightly shifted downfield CH_2−(Si) signal at δ 11.5 for the −$(CH_2)_3$SH moiety (Figure 1). This confirms the presence of mercaptopropyl groups anchored to the pore walls. Furthermore, IR spectra of **4** (x = 9) display a characteristic S−H stretching vibration of low intensity at 2575 cm^{-1}.[22] The N_2 adsorption/desorption isotherms of materials **1**−**4** are characteristic of mesoporous materials with a narrow pore size distribution (Figure 2).[23]

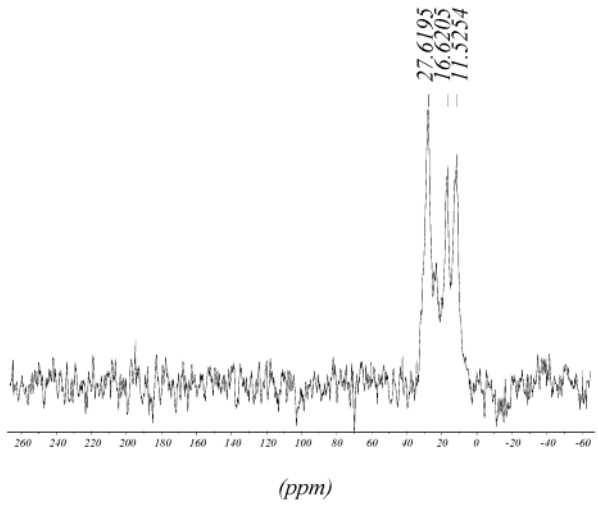

Figure 1. ^{13}C CP MAS NMR spectra of material **3**.

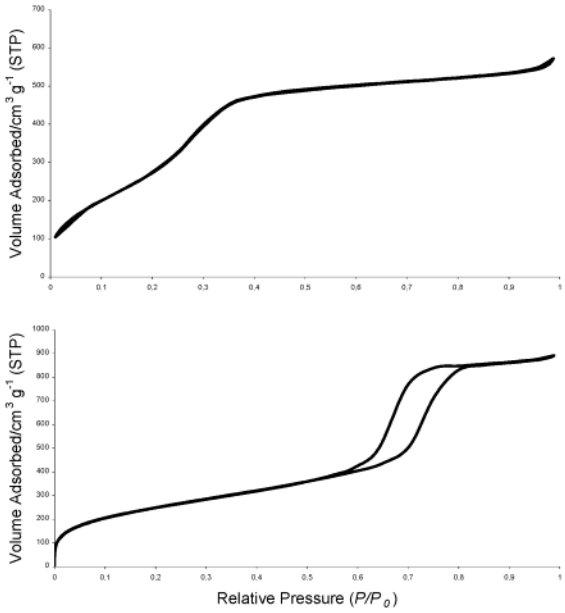

Figure 2. Nitrogen adsorption/desorption isotherms of **2** (top) and **3** (bottom).

High values ranging between 675 and 1055 m^2 g^{-1} for the Brunauer−Emmett−Teller[24] (BET) surface areas for

(21) Corriu, R. J. P.; Hoarau, C.; Mehdi, A.; Reyé, C. *Chem. Commun.* **2000**, 71. Corriu, R. J. P.; Mehdi, A.; Reyé, C. *C. R. Acad. Sci. Paris, Série IIc* **1999**, 35. Corriu, R. J. P.; Guari, Y.; Mehdi, A.; Reyé, C.; Thieuleux, C. *Chem. Commun.* **2001**, 763. Corriu, R. J. P.; Embert, F.; Guari, Y.; Mehdi, A.; Reyé, C. *Chem. Commun.* **2001**, 1116.
(22) Margolese, D.; Melero, J. A.; Christiansen, S. C.; Chmelka, B. F.; Stucky, G. D. *Chem. Mater.* **2000**, *12*, 2448.
(23) Gregg, S. G., Sing, K. S. W., Eds. *Adsorption, Surface Area and Porosity*; Academic Press: London, 1982.
(24) Brunauer, S.; Emmett, P. H.; Teller, E. *J. Am. Chem. Soc.* **1938**, *60*, 309.

1−**4** were obtained (Table 1). Pore size distribution was calculated from Barrett−Joyner−Hellenda (BJH) theory[25] on the basis of nitrogen adsorption/desorption measurements. The values obtained for the pore diameters are given in Table 1 as the maximum of the BJH pore size distribution calculated from adsorption and desorption curves. The low angle X-ray diffraction (XRD) patterns of the materials synthesized were characteristic of mesostructured phases (Figure 3). The expected wormlike[13] and hexagonal[20] structures were confirmed, respectively, for **1** and **3** by transmission electron microscopy (TEM) studies.

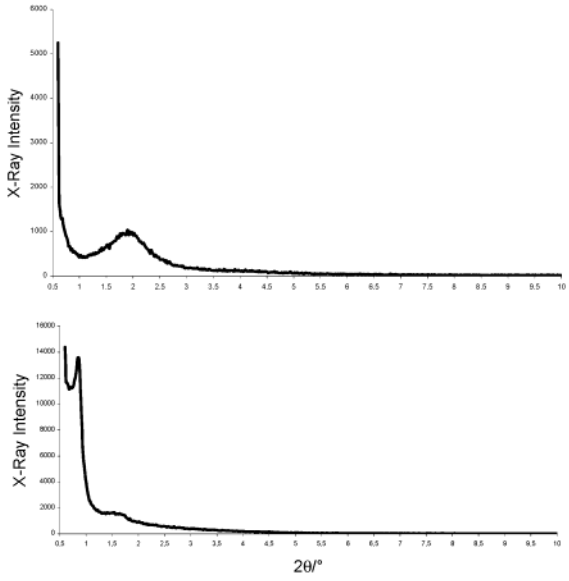

Figure 3. Powder XRD diffraction patterns for **2** (top) and **3** (bottom).

Gold Complexation and Nanoparticles Formation. Anchoring of gold within materials of type **1**−**4** was performed following two methods.

Method A is the well-known Turkevich method,[26] which uses hydrogenotetrachloroaurate (III) hydrate ($HAuCl_4 \cdot 3H_2O$) as organogold precursor, and method B is a new method using chloro (tetrahydrothiophene) gold (I) (AuCl(THT)) as organogold precursor. Both of them are described in the Experimental Section.

The solids obtained after this first step (anchorage of the organogold precursor) were named **($^{y}N_{x}$)** (see Scheme 2); where **y** indicates the conditions of anchorage of the organogold precursor (A for method A and B for method B), **N** specifies the starting material used for gold incorporation (**1**, **2**, **3**, or **4**), and **x** indicates the theoretical [Au]/[SR] ratio. Thus, from materials **1**−**4**, anchorage of gold with a ratio [Au]/[SR] = 0.2 gave rise to materials **($^{A}1_{0.2}$)**, **($^{A}2_{0.2}$)**, **($^{A}3_{0.2}$)**, and **($^{A}4_{0.2}$)** following method A, and **($^{B}2_{0.2}$)** and **($^{B}3_{0.2}$)** following method B.

After this first step (Scheme 2), gold content of these materials was inferred from the results of elemental analyses of Au, S, and Si. The BET surface area, pore volume, and pore size for materials **($^{y}N_{0.2}$)** decreased in comparison to the textural data of starting materials, which is consistent with pore filling (Table 1). An important textural modification of the HS−HMS-C_{16} type materials **1** and **2** treated according to method A to give **($^{A}1_{0.2}$)** and **($^{A}2_{0.2}$)** was observed at this stage, whereas there was no textural modification for material **2** treated following method B (material **($^{B}2_{0.2}$)**). This alteration consists of a shift of the pore size to higher values and an enlargement of the pore size distribution. It is worth noting that the same textural modification occurred when the HS−HMS-C_{16} type materials **1** and **2** were treated in the same way but in the absence of organogold precursor. Furthermore, no such textural modification was observed for HS−SBA-15 type materials **3** and **4**, whatever the method of anchorage of organogold precursor (A and B). Therefore, the textural modifications undergone by the HS−HMS-C_{16} type materials **1** and **2** during the anchorage of the organogold precursor according to method A were attributed to the poor hydrothermal stability of these materials (Figure 4).

Scheme 2. Preparation of the Gold (0) Nanoparticles-Containing Materials: Method A (i) $HAuCl_4 \cdot 3H_2O$, (ii) $HOC(CO_2Na)(CH_2CO_2Na)_2$; Method B (i) AuCl(THT), (ii) $Na(acac) \cdot H_2O$

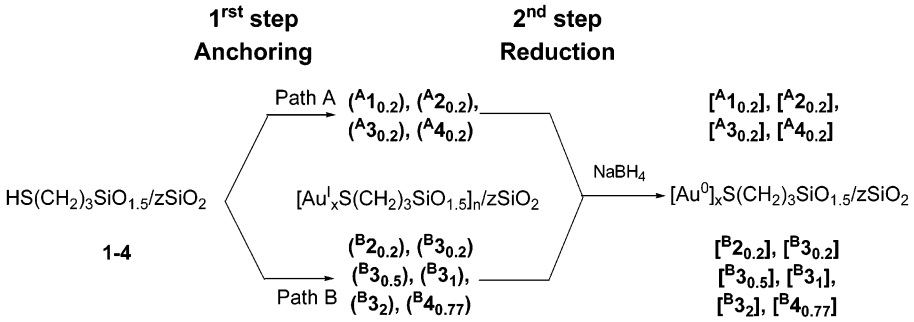

(25) Barrett, E. P.; Joyner, L. G.; Hallenda, P. P. *J. Am. Chem. Soc.* **1951**, *73*, 373.
(26) Turkevich, J.; Stevenson, P. C.; Hillier, J. *Discuss. Faraday Soc.* **1951**, *73*, 55.
(27) Marler, B.; Oberhageman, U.; Vortmann, S.; Gies, H. *Microporous Mater.* **1996**, *6*, 375.
(28) Templeton, A. C.; Wuelfing, W. P.; Murray, R. W. *Acc. Chem. Res.* **2000**, *33*, 27.

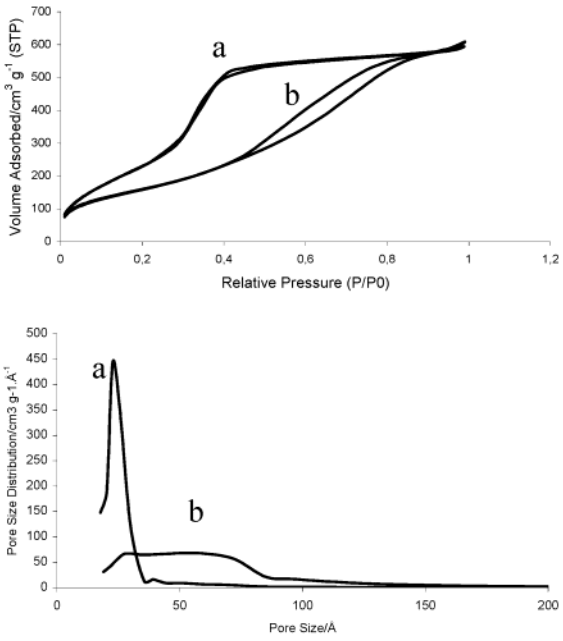

Figure 4. Nitrogen adsorption/desorption isotherms (top) and BJH pore size distribution (bottom) of **1** (a) and **[^{A}1$_{0.2}$]** (b).

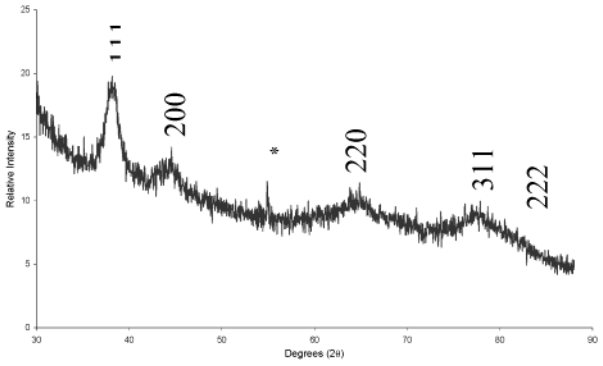

Figure 5. XRD pattern of **[^{A}1$_{0.2}$]**. (*) Indicated impurity attributed to boron silicate species.

In all cases, the X-ray diffractograms revealed a decrease of reflections from materials **1**−**4** to composite materials **(^{A}1$_{0.2}$)**, **(^{A}2$_{0.2}$)**, **(^{A}3$_{0.2}$)**, **(^{A}4$_{0.2}$)**, **(^{B}2$_{0.2}$)**, and **(^{B}3$_{0.2}$)**. This is a confirmation of the pore filling of the host material, which reduces the scattering contrast between the pores and the walls of the molecular sieves.[27]

For the materials **(^{y}N$_{0.2}$)** obtained after the first step (Scheme 2), neither observance of plasmon band absorbance in the UV−Vis spectrum nor diffraction peaks in the X-ray diffractograms characteristic of gold (0) nanoparticles-containing materials were observed, whatever the method followed.

TEM images show weakly contrasted particles with sizes less than 1.5 nm. These particles, the size of which is not dependent on the host material pore size, were attributed to formation of an $(-Au^{I}SR-)_n-$ polymer.[28] Therefore, these colorless solids **(^{y}N$_{0.2}$)** were treated with an ethanolic sodium borohydride ($NaBH_4$) solution at 60 °C for 24 h (step 2, Scheme 2) giving rise to purple solids, after filtration and drying (see Experimental Section). The solids obtained after $NaBH_4$ treatment were named **[^{y}N$_{0.2}$]** to distinguish them from the materials **(^{y}N$_{0.2}$)** obtained before treatment with $NaBH_4$.

Slight decreases in BET surface area and pore volume were observed (Table 1) for the materials **[^{y}N$_{0.2}$]** in comparison to materials **(^{y}N$_{0.2}$)**.

All the materials **[^{y}N$_{0.2}$]** exhibited intense plasmon band absorbance at 520 nm, indicative of gold (0) nanoparticles. The XRD pattern of **[^{A}1$_{0.2}$]** (Figure 5) displayed for the high angle region ($2\theta = 20-70$) broad reflections characteristic of gold (0) nanoparticles. For the materials **[^{y}N$_{0.2}$]**, ([Au]/[SR] = 0.2), the gold (0) nanoparticles size derived from TEM measurements are in good agreement with the pore size values obtained from BET measurements whatever the method followed, taking into account the experimental errors (Figures 6 and 7a). TEM photographs clearly show a single distribution even for **[^{A}1$_{0.2}$]** and **[^{A}2$_{0.2}$]** materials obtained respectively from **1** and **2** following method A. However, in both cases, the large size distribution observed results from the modification of the silica matrix during the first step of the process. A narrower size distribution was obtained for the gold (0) nanoparticles included in materials, **[^{A}3$_{0.2}$]**, **[^{A}4$_{0.2}$]** (Figure 6), and **[^{B}3$_{0.2}$]**, whatever the method adopted (Method A or B). However, the presence of gold (0) nanoparticles could not be demonstrated by TEM, UV−Visible, or XRD measurements for material **[^{B}2$_{0.2}$]**. In this case, the diffusion of the reducing agent is probably difficult if one considers the pore size of these materials (24 Å). Another explanation could be the very small size of the as-obtained particles, which rendered their characterization difficult by the techniques used.

To confirm the anchoring role of the thiol functions, we increased the ratio [Au]/[SR] step-by-step from 0.2 to 2. This series of experiments was performed following method B using the HS−SBA-15 material **3**. Anchorage of gold with [Au]/[SR] ratios of 0.5, 1, and 2 led, respectively, to materials **(^{B}3$_{0.5}$)**, **(^{B}3$_{1}$)**, and **(^{B}3$_{2}$)**, which after the reduction step gave rise to materials **[^{B}3$_{0.5}$]**, **[^{B}3$_{1}$]**, and **[^{B}3$_{2}$]**, respectively (Figure 7b). For material **(^{B}3$_{0.2}$)** with [Au]/[SR] = 0.2, and as for material **(^{B}3$_{0.5}$)** with [Au]/[SR] = 0.5, no nanoparticles formation was observed at the first step of the process. In these cases, the amount of thiol present in the solid allows the stabilization of the entire organogold precursor in the form of the polymer $(-Au^{I}SR-)_n$. In contrast, when [Au]/[SR] ≥ 1 (materials **(^{B}3$_{1}$)** and **(^{B}3$_{2}$)**), outer pore growth of nanoparticles was observed after the addition of the organogold precursor. For [Au]/[SR] = 1, even if the necessary amount of thiol for stabilization of the organogold precursor is present, because of diffusion and/or accessibility problems in the experimental conditions used, outer pore growth of nanoparticles was observed but only in small quantities. For [Au]/[SR] = 2, the excess of organogold precursor, which could not be stabilized by the thiol functions, gave rise to the formation of nanoparticles at the surface of the grains in large quantities. This is consistent with the necessity of the complexation of the organogold precursor onto the thiol function prior to chemical reduction in order to control the size distribution of the as-obtained nanoparticles. Furthermore, these thiol func-

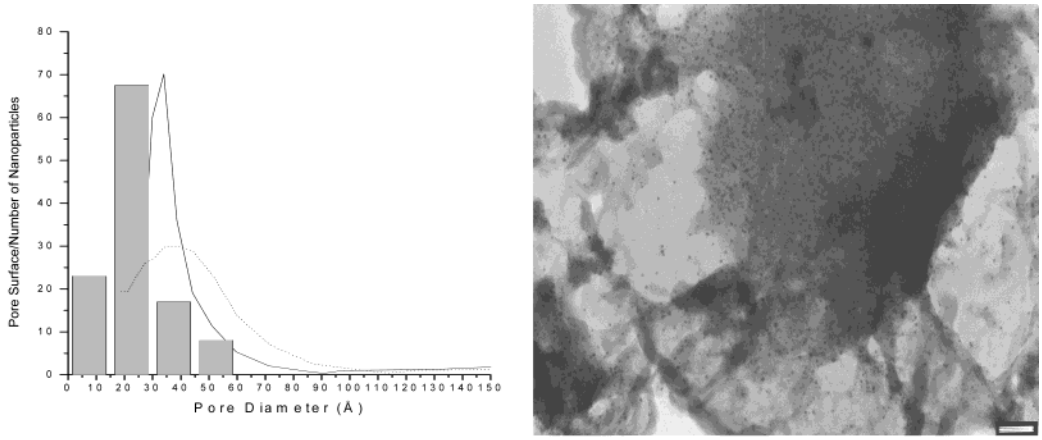

Figure 6. Left: Correlation between the pore diameter (solid/dotted lines for adsorption/desorption data from N_2 studies) and the gold (0) nanoparticles size (columns) for **[^{A}4$_{0.2}$]**. Right: TEM image of a replica of material **[^{A}4$_{0.2}$]**. Scale bar: 50 nm.

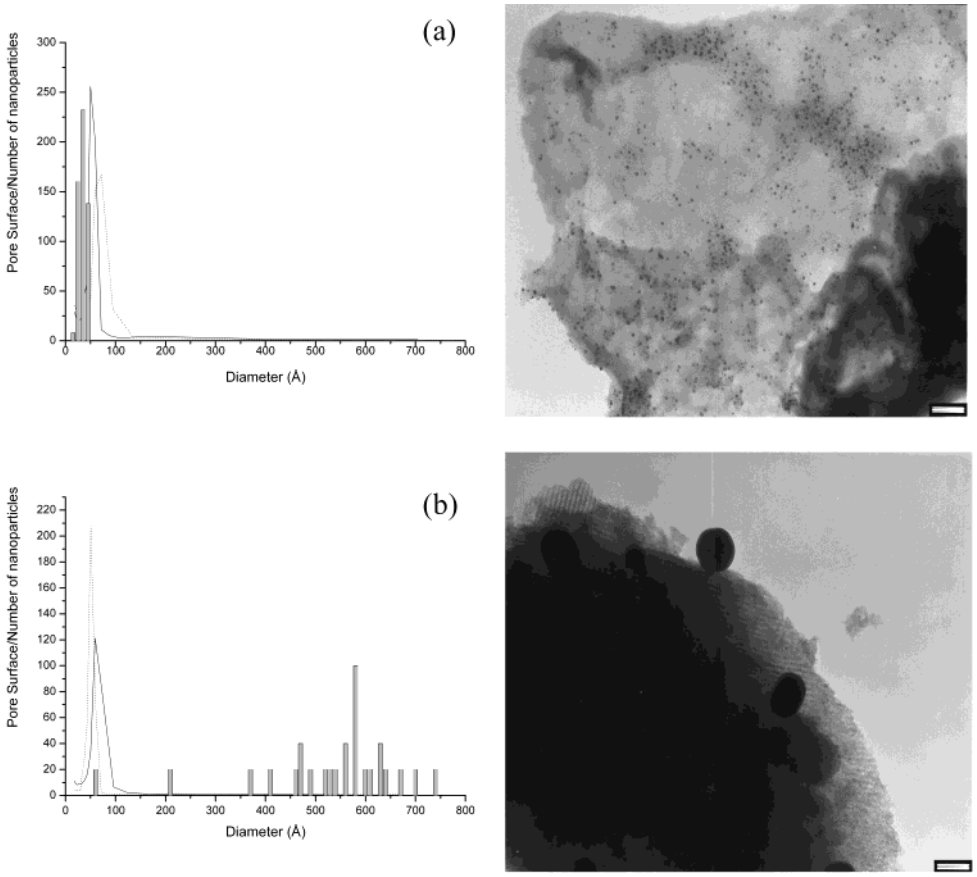

Figure 7. Left: Correlation between the pore diameter (solid/dotted lines for adsorption/desorption data from N_2 studies) and the gold (0) nanoparticles size (columns) for (a) **[^{B}3$_{0.2}$]** and (b) **[^{B}3$_{2}$]**. Right: TEM photographs representative of materials (a) **[^{B}3$_{0.2}$]** (replica) and (b): **[^{B}3$_{2}$]**. Scale bar: 50 nm.

tions interact strongly with the gold nanoparticle surface, which retains the nanoparticles within the pores. Considering these results, we prepared material **(^{B}4$_{0.77}$)** with a ratio [Au]/[SR] = 0.77 from material **4** following method B, giving rise to material **[^{B}4$_{0.77}$]** after reduction step.

The organogold precursor was stirred in the presence of material **4** for 48 h to allow complete diffusion within the channels before isolation of material **(^{B}4$_{0.77}$)**. $NaBH_4$ was added to a suspension of this material and stirred for 48 h to obtain complete reduction and avoid the presence of residual gold polymer particles. Material

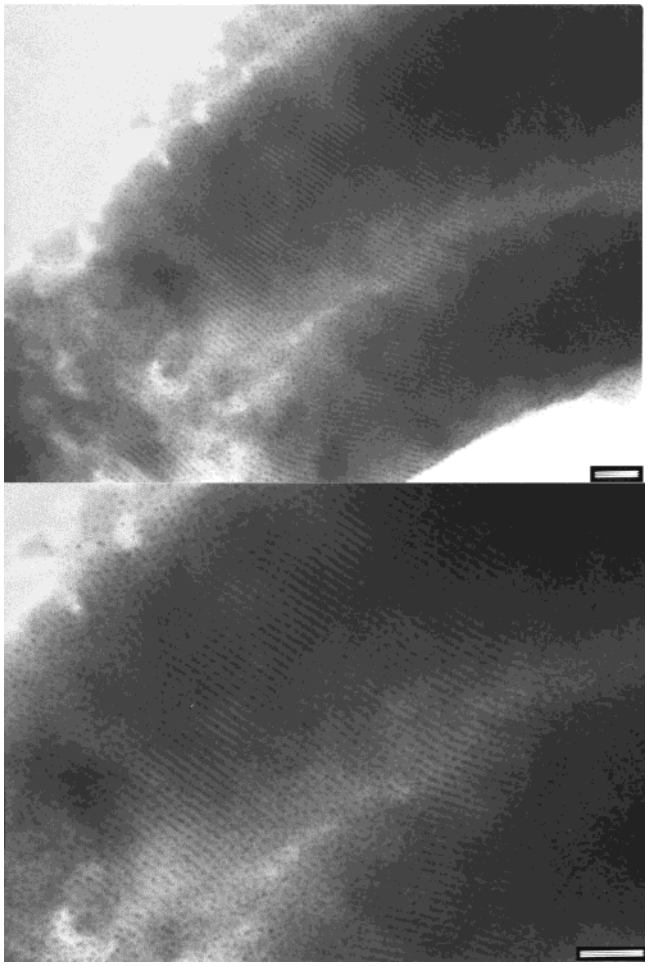

Figure 8. TEM images of **[$^{B}4_{0.77}$]**. Scale bar: 50 nm.

[$^{B}4_{0.77}$] containing 16.1wt % of gold as given by elemental analysis displays a high density of nanoparticles located exclusively within the channels of the mesoporous material, as can be seen from TEM measurements (Figure 8).

Conclusion

We report here the preparation of gold (0) nanoparticles within channels of mesoporous materials functionalized with mercaptopropyl groups. These materials prepared using the so-called direct method contain various and controlled numbers of thiol functions, which are homogeneously distributed exclusively within the pore channels. The regular distribution of organic groups allows the exclusive growth of nanoparticles with a narrow size distribution within the pores of the materials with gold content as high as 16.1 wt %. The good control of size distribution of the nanoparticles obtained, due to their exclusive location within the channels of the materials, demonstrates the crucial role of the thiol functions both for (i) the complexation of the organogold precursor prior to the reduction step, and (ii) for their strong interaction with the gold nanoparticle surface during and after the nanoparticle growth process.

Acknowledgment. We thank the CNRS and the Université de Montpellier II for financial support. C.T. thanks Air Liquide for a grant. S.G.G. thanks EU, TMR network CLUPOS for a grant.

Supporting Information Available: Graphs of correlation betwwen pore diameters and gold (0) nanoparticles size, and TEM images of materials (PDF). This material is available free of charge via the Internet at http://pubs.acs.org.

CM0213218